Hydrodynamic Performance and Acoustic Response of Ship Propeller

Srinivas Prasad Sanaka[a], Pardhasaradhi N[a], Durga Rao K[b]

The aim of the paper is to predict the hydrodynamic performance and noise generated by the propeller at different advance ratio and the speed of the propeller. Three bladed, DTMB 4119 propeller model was created using the NACA66 modified line, a = 0.8 hydrofoil profile. ANSYS Workbench software is used for mesh generation and computational analysis. A large-eddy simulation turbulence model and Ffowcs Williams-Hawkings (FWH) acoustic model is used for all simulations. A moving reference frame is used to simulate the rotational effects of the propeller. The speed of the propeller is 792 rpm, the propeller being 0.2 m, and inlet velocity is varied to study the effect of the advance ratio. A transient analysis is carried out using a time step value of 0.0005 seconds and the total simulation time is 0.6 seconds. The hydrodynamic performance parameters are validated by comparing with the experimental data available in the literature. The sound pressure level (SPL) is plotted over the frequency range of 0 to 1000 Hz at different locations, speed, and an advance ratio of 0.5, 0.7, 0.833, and 0.9,1. The structural, acoustic and hydrodynamic behaviour of the propeller was predicted using a two-way fluid structure interaction at an advance ratio of 0.833. The major conclusions drawn from the analysis are that the sound pressure level values are increased at the propeller off-design conditions and varying with the receiver locations. The data generated from this study is useful for the designers to carry out further research in order to reduce the noise generated from the propeller.

KEY WORDS
~ Hydrodynamics
~ Propeller
~ CFD
~ Numerical analysis
~ Acoustics
~ Advance ratio

a. V.R. Siddhartha Engineering College, Department of Mechanical Engineering, Vijayawada, India

e-mail: drssp1974@gmail.com

b. Adikavi Nannaya University, University College of Engineering, Department of Mechanical Engineering, Rajamahendravaram, India

doi: 10.7225/toms.v12.n01.001

This work is licensed under CC BY

Received on: Mar 21, 2022 / Revised on: Aug 7, 2022 / Accepted on: Jan 3, 2022 / Published: Apr 20, 2022

1. INTRODUCTION

The marine propeller produces the required thrust to push the ship in the forward direction. The hydrodynamic performance of the propeller at different advance velocities is important for the designer and at the same time the noise generated from the propeller during its operation should be less from the stealth technology point of view. The location of marine vessel and its velocity can be detected by the enemies based on the propeller noise. (Stuart Dodge Jessup, 1989) measured the hydrodynamic performance of 0.3 diameter DTMB 4119 propellers. (Pan Y et al., 2013; Seol et al., 2005; Bagheri et al., 2014), studied the acoustic effects, and the acoustic spectrum was plotted for different operating conditions. (Kai Abrahamen, 2012) described the propeller noise, machinery noise, and flow noise. Batool Mousavi et al. (2014) computed the hydrodynamic noise generated by the three-bladed, 0.3048m diameter, DTMB 4119 propeller using the Open FOAM software around. However, the sound pressure level is plotted in the range of 0 to 150 Hz at a speed of 120 rpm, the conclusion being that an increase in the acoustic pressure range of the noise is compatible with a decrease in advance coefficients. (Thomas Lloyd et al., 2015) studied the hydrodynamic performance of 0.227m, a four-bladed, INSEAN E779A propeller,

using ReFRESCO CFD code and a sound pressure variation with the pertaining frequency was plotted for RANS and FWH models. (Woen-Sug Choi et al., 2015) predicted that the noise generated by the cylinder using ANSYS Fluent software and sound pressure level was plotted in the frequency range of 0 to 1000 Hz. (Bagheri. et al. 2015) studied the hydrodynamic and noise levels on two four- bladed propellers, similar to DTMB 4119 propeller. The sound pressure level is plotted at the receiver points, considered in radial and downstream directions. SPL values decreased with the increase of the distance of the location of the receiver points, both radially and axially. The sound pressure level decreased with an increase in frequency range. (Boumediene K and Belhenniche S.E, 2016) computed the hydrodynamic performance parameters of 0.3048m DTMB 4119 marine propeller, using RANS turbulent model, also employing commercial ANSYS Fluent software. (Savas Sezen et al. 2017) studied the effect of cavitation and propeller rotation on the acoustic performance of the three-bladed, 0.3048m diameter DTMB 4119 propeller. The SPL values are plotted against the rotational speed of the propeller advance ratio. A decrease in the sound pressure level was observed with an increase in advance ratio, and quite the opposite trend was observed with the speed of the propeller. (Lidtke, 2017) studied the cavitation characteristics of 0.25m diameter, five-bladed, VP1304 Potsdam propeller. Open FOAM software was used for the hydrodynamic and cavitation studies. The test results of sound power spectral density were plotted in the frequency range of 0 to 10000 Hz. (Gorji Mohsen et al., 2017) studied the hydrodynamic and acoustic effects on four-bladed, 2.1 m diameter, using ANSYS Fluent software. The LES and DNS turbulence models gave a better solution at the nearest wall.

(Abouzar Ebrahimi et al., 2019) predicted the hydrodynamic performance coefficients of 0.2 m diameter DTMB 4119 marine propeller and the noise generated by the propeller using panel method at an advance ratio of 0.833. (Boumediene et al., 2019) have estimated the hydrodynamic thrust and moment coefficients generated by Seiun Maru propeller using ANSYS Fluent software between the advance ratio values from 0.1 to 1. (Goutam Kumar Saha et al. 2019) predicted the hydrodynamic performance of the four-bladed, 1.6m diameter, B-series marine propeller, using commercial software, concluding that the thrust coefficient (KT) and torque coefficient 10 (KQ) increased with the decrease in the advance ratio (J). (Hai-peng Guo et al., 2019) computed the hydrodynamic performance of ONRT propeller and DTMB 5415 marine propeller. (Fatima Bouregba et al., 2019) studied the hydrodynamic performance of Wageningen B series four, five, and six-bladed propellers, using ANSYS Fluent software, coming to a conclusion that the performance of six-bladed propeller was good. (Ahmet Soydan et al. 2019) studied the hydro-acoustic performance of three-bladed, 0.3048 m diameter DTMB 4119 propeller.The acoustic performance of the propeller was computed using CFD software by varying the blade number and the diameter of the propeller. It was concluded that the sound pressure level increases with the blade number and diameter of the propeller. The diameter of the propeller is the parameter most influencing the propeller noise, much more than the blade number of the propeller. The sound pressure level is plotted only in the range of 0 to 500 Hz. The sound pressure level values were also calculated by using the semi-empirical Brown's formula. (Yuhang Wu et al., 2019) studied the acoustic characteristics of the two-bladed, 1.6 m diameter propeller. The noise generated by the propeller is predicted for the speeds of 500 rpm, 1000 rpm, 1500 rpm, 2000 rpm, and 2200 rpm. It was established that the noise level increased with the increase in speed of the propeller. The noise level generated by the propeller decreased with the blade shape modification along the span wise. (Savas Sezen and Sakir Bal, 2019) investigated the performance of 0.3048m diameter DTMB 4119 propeller and the noise spectrum for two, three, and four-bladed propellers were compared, the conclusion being that the noise level decreases with an increase in blade number. Several researchers published the hydrodynamic performance of the propellers. A systematic study on the noise prediction for various operating conditions on 0.2 m diameter DTMB 4119 propeller is not available in the literature. The aim of this paper is to investigate the hydrodynamic and acoustic behaviour of the propeller at different advance ratios, rotational speed, and locations of the receiver points in fluid domain.

2. MODEL AND FLUID DOMAIN CONSIDERED FOR ANALYSIS

2.1. Model Selected for Analysis

The DTMB 4119 propeller geometry was chosen from Abouzar Ebrahimi et al. (2019) for the validation and

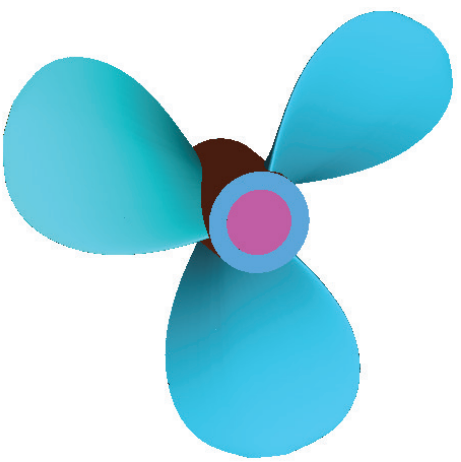

Figure 1.
DTMB 4119 propeller.

computational analysis, while the propeller geometry parameters available in the literature are used to generate the propeller. ANSYS Workbench software was used and three dimensional propellers were generated. Three-bladed DTMB 4119 propeller of 0.2 m diameter is shown in Figure1. NACA 66 modified (a = 0.8) profile is used in each blade section.

2.2. Mesh Used in Fluid Domains

Computational domain measurements are expressed in terms of the diameter of the propeller and are depicted in Figure 2. The diameter of the outer fluid domain is 8D. The inlet location is at a distance of three times the diameter of the propeller from the propeller, and the outlet location is four times the diameter of the propeller. There are two fluid domains. One is for external flow on rotating propeller, and the other is to apply the moving frame of reference, in which fluid rotation is assigned to the rotational speed of the propeller. Tetrahedral elements were used in both the fluid domains and meshes were generated in ICEM CFD software. Tetrahedral elements were also used in fluid and solid domains due to the complexity in geometry. The tetra mesh generated on the propeller is depicted in Figure 3. The mesh in the moving frame of reference zone around the propeller is shown in Figure 4.

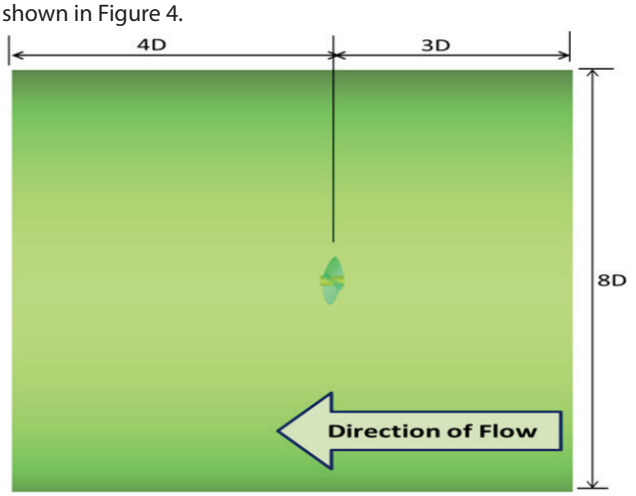

Figure 2.
Fluid domain around the propeller.

Very small size tetrahedral elements are used as the tip of the propeller. Smaller elements are used at the trailing edge location of the propeller blade to maintain good quality in the process of mesh generation. The mesh generated in the external

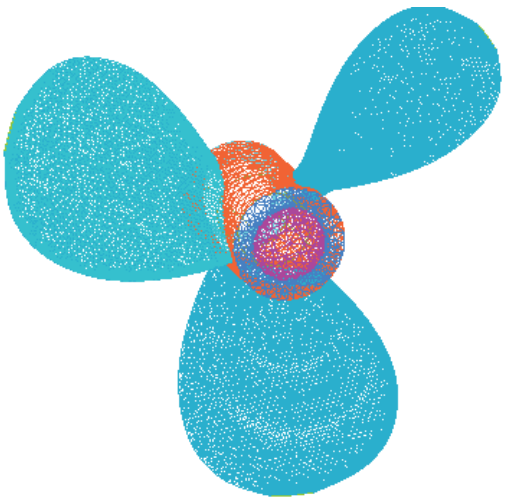

Figure 3.
Mesh on the propeller domain.

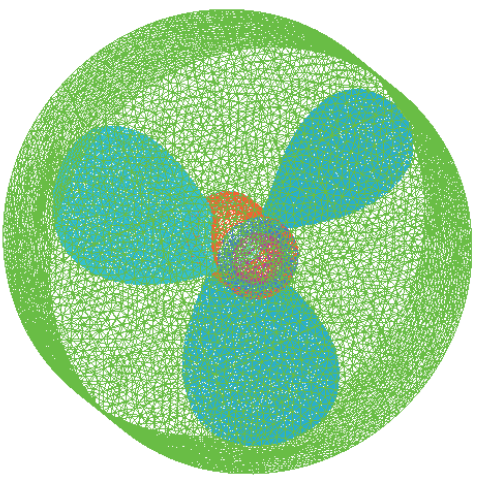

Figure 4.
Mesh in rotating.

fluid domain is illustrated in Figure 5. The number of elements used in the fluid domains for transient fluid flow analysis is 1.33 Million. Tetrahedral elements are used in the location of the propeller hub. Number of elements in solid blades is 324921 and in hub is 126564. The total number of elements in solid domain is 451485.

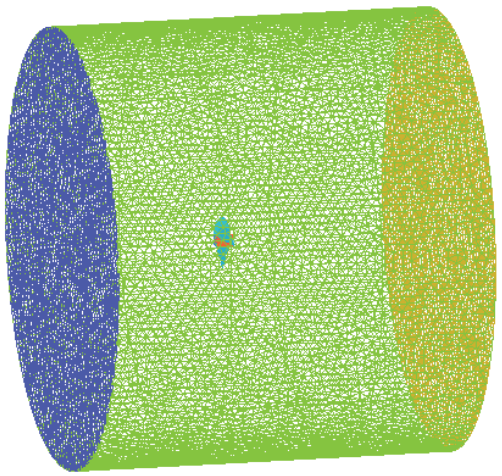

Figure 5.
Mesh in stationary fluid domain.

2.3. Grid Independence Study

The performance parameters of the propeller were computed by varying the number of elements from 0.42 to 1.368 million. The variation of thrust and moment coefficient with the number of elements is plotted in Figure 6 and these values at 1.33 and 1.68 million are close to the experimental data. The computational time taken to carry out the two way fluid structure interactions with 1.33 million elements is 48 hours using Dell-Intel I-7 processor with 16 GB Ram and 4TB hard disk. Therefore the number of elements selected for the computational analysis in fluid domain is 1.33 million.

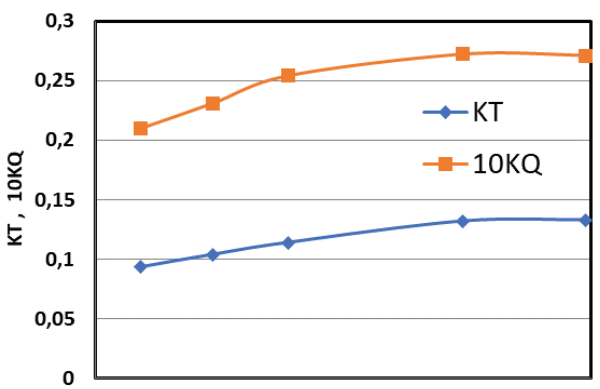

Figure 6.
Grid independence study.

3. SOLVER PARAMETERS USED FOR COMPUTATIONAL ANALYSIS

This time step value is calculated using the equation (1) to plot the acoustic pressure level in the range of 0 to 1000 Hz. f value, as defined in the equation is 1000 Hz. The calculated time step value is 0.0005 seconds used for transient analysis.

$$\Delta t = \frac{1}{2t} \quad (1)$$

A pressure based solver is used for the transient simulations. The large eddy simulation model is used to capture the turbulence effects, and Ffowcs Williams Hawkings(FWH) acoustic model has been defined to simulate the acoustic effects. The water density used is 1026 kg/m3 for all simulations and water viscosity used is 0.001003 kg/m-s. Rotation is assigned to the fluid around the propeller and is rotated with 792 rpm in order to use the moving reference frame (MRF) approach. The simulations are carried out at an advance ratio of 0.5, 0.7, 0.833, 0.9, 1. The advance velocity magnitude, defined for advance ratio 0.833, is 2.22 m/s. The surface existing between the rotating domain and the stationary domain is used as interior. The advanced velocity is defined at the inlet, and the pressure outlet boundary condition is used at the outlet of the domain, whereas 0 Pascal is the magnitude of pressure defined at the outlet. The operating pressure is 101325 Pascal. External surfaces of the propeller are defined as a source zone type wall. The reference acoustic pressure used for acoustic pressure calculation is 1e-6. Far field sound speed defined is 1500 m/s, and the acoustic source surface is represented by the total surface of the propeller blades.

4. RESIDUALS

The continuity, x-velocity, y-velocity, and z-velocity residuals are plotted against the number of iterations in Figure7. The residual plots become flat curves at 4800 iterations. The residual target defined is 10-9 , and the continuity residual is in the range of 10-4. The residuals are diminishing gradually with the number of iterations before 4,800 iterations.

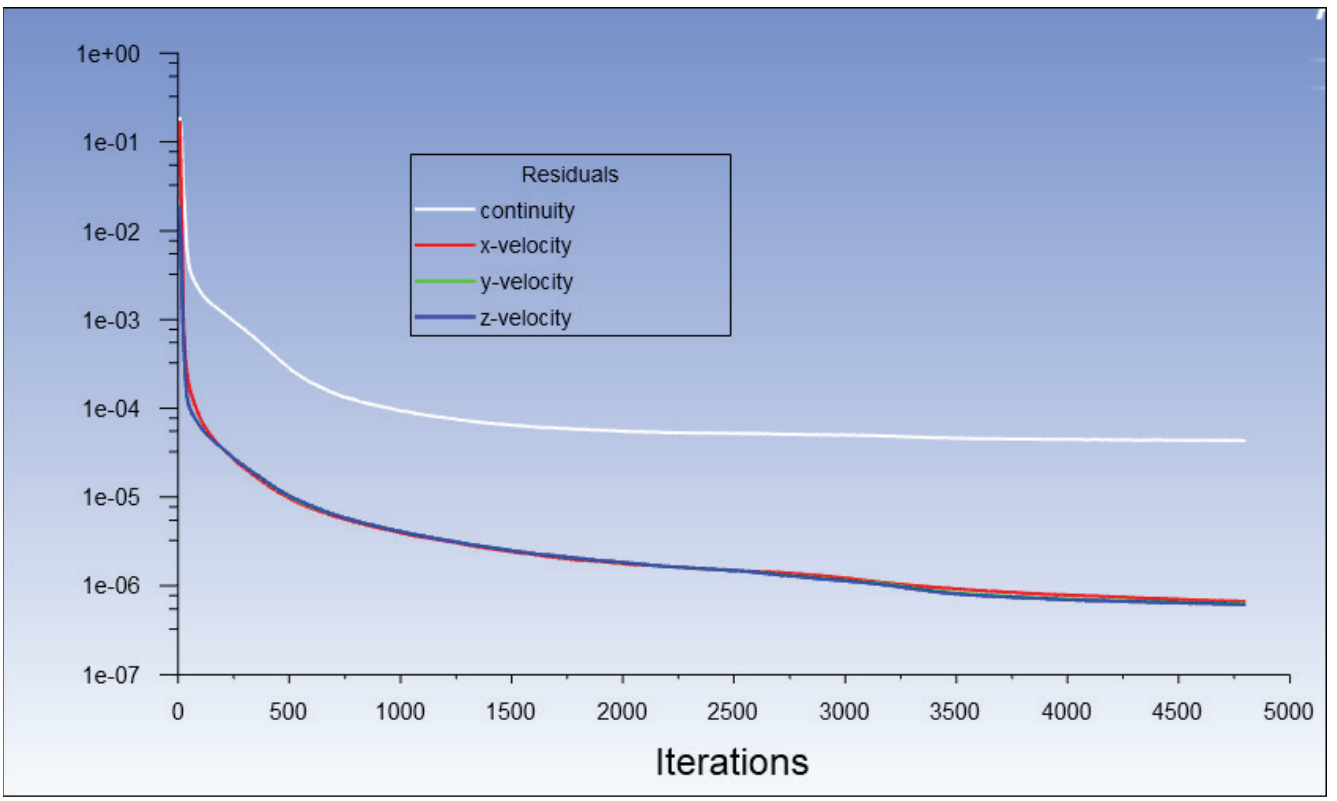

Figure 7.
Residuals plot.

5. RESULTS AND DISCUSSION

5.1. Hydrodynamic Performance Parameters

In this study thrust coefficient, moment coefficient and efficiency have been computed, using equations (2), (3) and (4) respectively.

$$K_T = \frac{T}{\rho n^2 D^4} \tag{2}$$

$$K_Q = \frac{Q}{\rho n^2 D^5} \tag{3}$$

$$\eta = \frac{1}{2\pi} \frac{K_T}{K_Q} \tag{4}$$

The advance velocity has been varied from 0.5 to 1.1m/s, and the speed of the propeller maintained constant at 792 rpm. The computational results shown in Figure 8 are thrust coefficient, torque coefficient, and efficiency in close agreement with the experimental data published by Abouzar Ebrahimi et al. (2019). The efficiency of the propeller is lower at a low advance ratio, and also lower at a high advance ratio, but maximum in design condition. The propeller hydrodynamic performance has proved poor in off-design conditions.

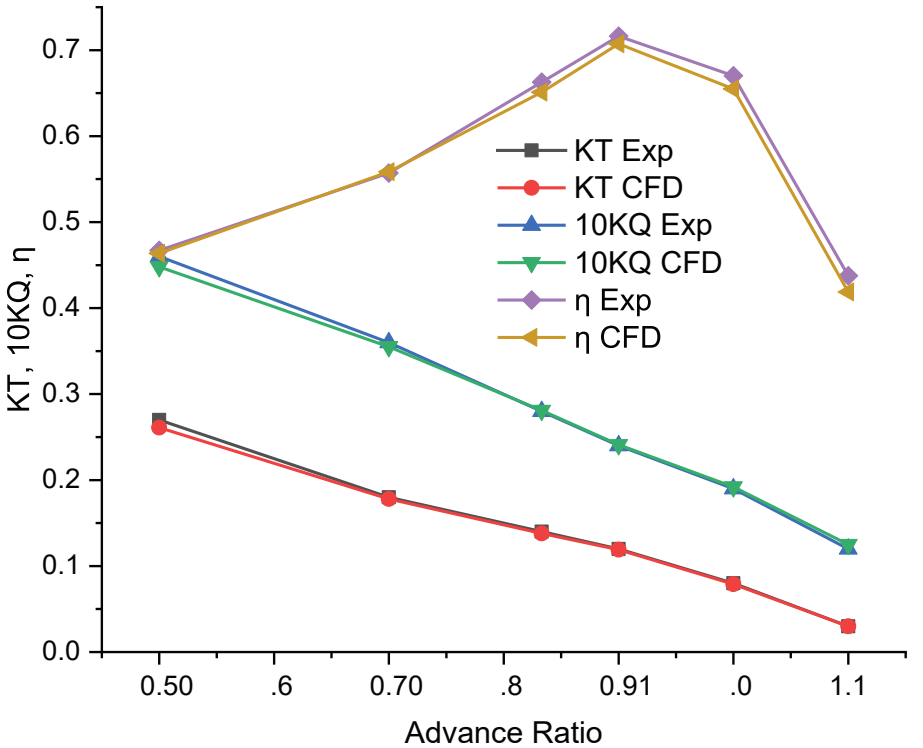

Figure 8.
Variation of hydrodynamic performance parameters with J.

5.2. Effect of Advance Ratio on Noise Prediction

The predicted sound pressure level (SPL) is plotted in the frequency range of 0 to 1000 Hz in Figure 9 at an advance ratio of 0.5, 0.7, 0.833, 0.9, 1. The location of the receiver point considered to plot the SPL data is at a distance of 0.595m from a propeller location in the downstream direction, and 0.255m in radial direction. The location of the receiver point is illustrated in Figure 10. The exponential decreasing trend of sound pressure level in the considered frequency range has been observed at all advanced ratios. It has also been observed that the SPL values at J = 0.5, 1 are high compared with other values. Total time for transient fluid flow analysis is 0.6s. Time step used is 0.0005s. The number of sub steps used in each time step is two. The average SPL values at each advance ratio have been illustrated in Figure 11. This plot indicates that the SPL at J =1 is 96 dB, whose maximum is at J=0.5, SPL is 93 dB. It is evident that, in off-design conditions, the sound generated from the propeller is high.

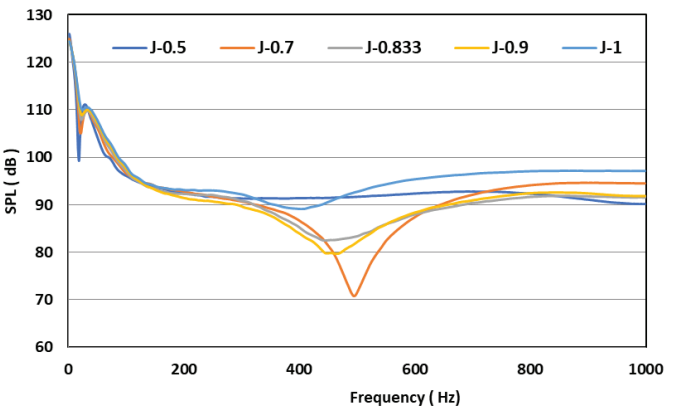

Figure 9.
Noise spectrum predicted at different advance ratios.

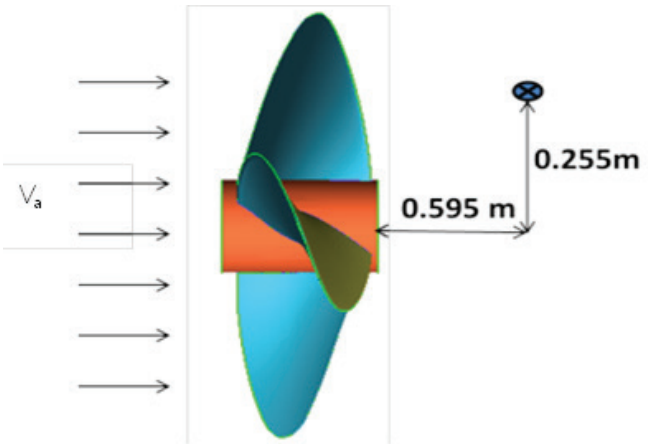

Figure 10.
Location of receiver point considered to plot SPL at different advance ratios.

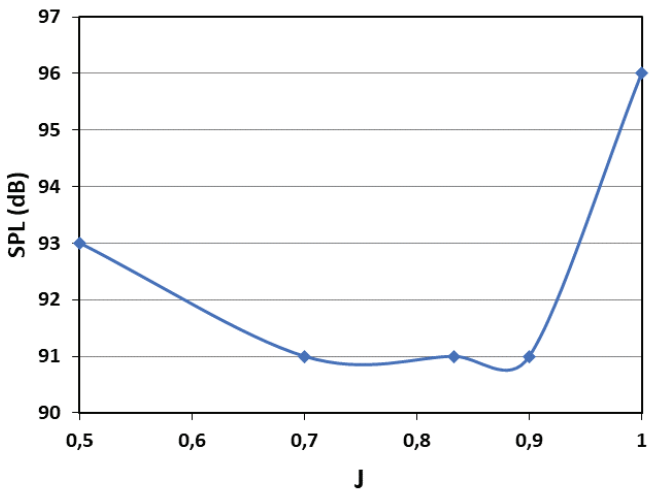

Figure 11.
Average SPL values at different advance ratios.

5.3. SPL at Different Locations of Receiver Points

The SPL is plotted at four locations in the frequency range of 0 to 1000 Hz in at J = 0.833 and is illustrated in Figure 12. The location of receiver point 2 is considered along the axial direction at a distance of 0.75m behind the propeller. The receiver 3 and 4 are perpendicular to each other and located at a distance of 0.75m from the center of the propeller in radial direction. The SPL values and the trend are same for the receiver 3 and 4. However, the plotted trend and magnitude of the SPL is different for receiver 1 and 2.

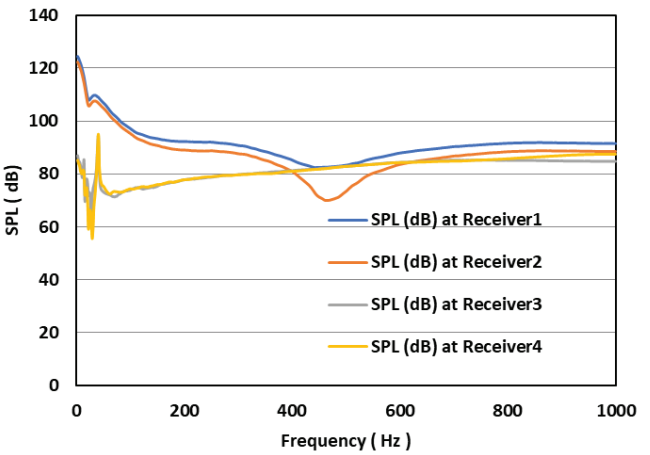

Figure 12.
Noise predicted at different location of receiver points at J = 0.833.

5.4. Effect of Rotational Speed

The operating conditions used for the noise prediction are given in table 1. The noise predicted over the frequency range from 0 to 1000 Hz has been plotted in Figure 13 at various speeds. It has been observed that the acoustic spectrum plotted at 400 rpm is lower compared with other speeds at the same advance ratio. The rotating speed of the propeller affects the noise generated by the propeller. The noise predicted is increasing with an increase in rotational speed of the propeller. The predicted sound pressure level distributions over the frequency at different speeds follow the same trend, as predicted by (Ahmet et al., 2019 and Yuhang Wu et al., 2019). The maximum value of SPL at 400 rpm is 117 dB, whereas at 1200 rpm it is 129 dB. The minimum value of SPL at 400 rpm is 58 dB, whereas at 1,200 rpm it is 98 dB. The variation of hydrodynamic characteristic performance parameters with the pertaining speed is illustrated in Figure 14. It has been observed that the thrust coefficient, torque coefficient, and efficiency values are almost the same for the selected operating conditions. Therefore, the propeller hydrodynamic performance is not affected by the operating conditions selected at an advance ratio 0.833. It can be concluded that there is no influence of rotational speed on the hydrodynamic performance of the propeller at different advance velocities and rotational speeds for the same advance ratio. It can consequently be recommended to operate the propeller at 400 rpm, 0.833 advance ratio in order to obtain the same performance with low noise levels.

Table 1.
Speed and advance velocity variation at J = 0.833.

	Advance ratio	Speed (rpm)	Advance velocity (m/s)
Case 1	0.833	400	1.11
Case 2	0.833	600	1.67
Case 3	0.833	792	2.22
Case 4	0.833	1000	2.78
Case 5	0.833	1200	3.33

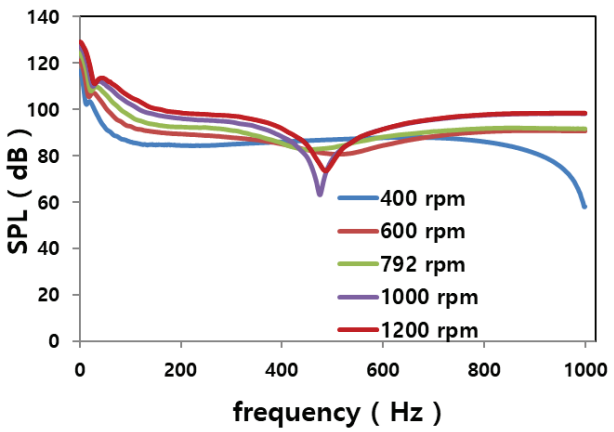

Figure 13.
Noise predicted at different speeds of the propeller at J = 0.833.

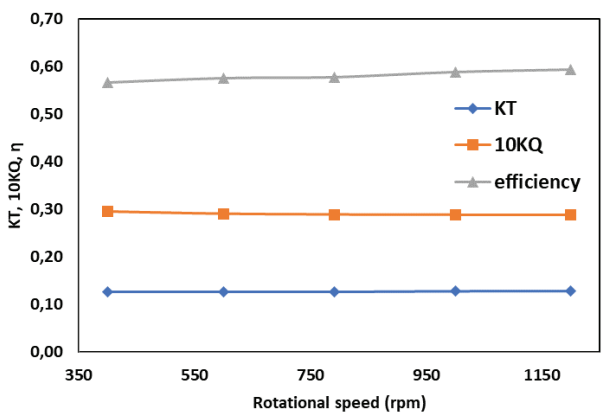

Figure 14.
Effect of the propeller speed on Hydrodynamic performance.

5.5. Structural Behaviour of the Propeller

Two-way fluid structure interaction analysis predicts the structural response, hydrodynamic performance, and the acoustic response of the propeller simultaneously. The structural data is transferred to fluid flow solver and vice versa during each time step. Two-way fluid structure interaction analysis is carried out at 0.833 advance ratio, and the stress induced in the propeller and total deformation of the propeller at a simulation time of 6 seconds is shown in Figures 15 and 16. Nickel-aluminum bronze alloy is the propeller material used for the structural analysis. The total time for a two-way analysis is six seconds.

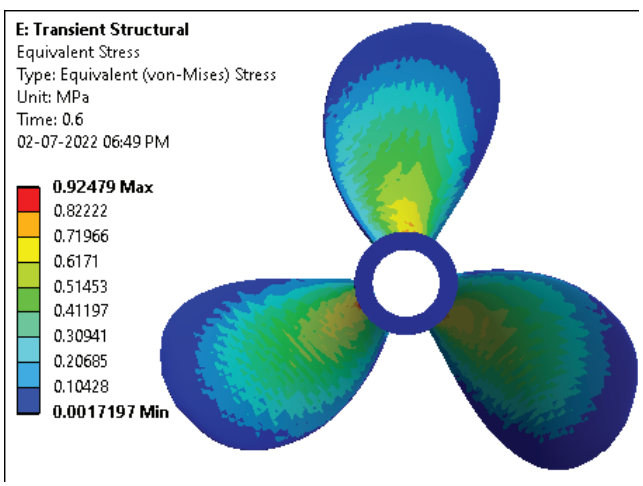

Figure 15.
Von-Mises stress induced in the propeller.

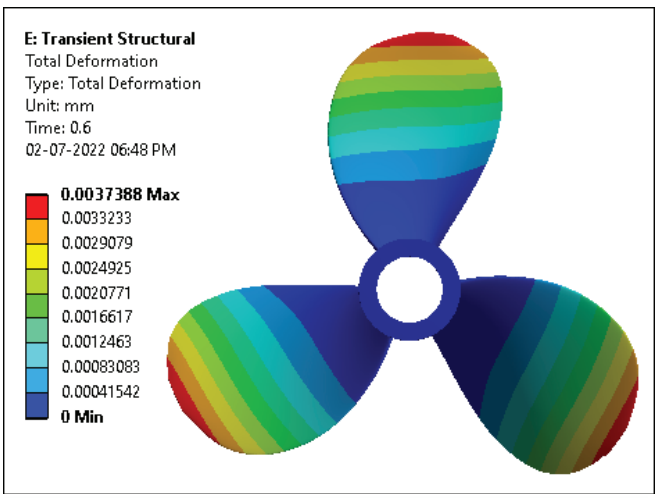

Figure 16.
Total deformation of the propeller.

6. CONCLUSIONS

Thrust coefficient, Torque coefficient, and efficiency at different advance ratios have been computed from the transient fluid flow analysis on 0.2 m diameter propeller, and the acoustic characteristics at different locations and advance ratios have been analyzed. The conclusions drawn from the computational analysis are as follows:

1. The computed thrust coefficient, moment coefficient, and efficiency are validated with the experimental results published in the literature;

2. The thrust coefficient and moment coefficient decrease with an increase in advance ratio;

3. The efficiency in off-design conditions is poor;

4. The acoustic characteristics of the propeller have been analysed, the conclusion being that the sound level predicted in off-design conditions is relatively high;

5. The sound pressure level is same for the receiver points considered at the same radius in the circumferential plane, the characteristics also being similar;

6. The sound pressure level varies from location to location within the fluid domain;

7. The propeller noise increases with the rotational speed;

8. The propeller noise predicted is low at a propeller speed of 400 rpm, without affecting the performance of the propeller;

9. This study may be useful to understand that any design modifications the of propeller are required in order to reduce the magnitude of the sound pressure level;

10. The acoustic data computed on the propeller provide comprehensive data for the propeller acoustics research area.

CONFLICT OF INTEREST: No potential conflict of interest has been declared by the author(s).

ACRONYMS

D	Diameter of the propeller (m)
η	Efficiency
f	Frequency (Hz)
J	Advance ratio
KT	Thrust coefficient
KQ	Torque coefficient
Q	Torque (N-m)
ρ	Density of water (kg/m^3)
T	Thrust force (N)
Δt	Time step size (s)
n	Propeller rotational speed (rps)
Va	Flow speed at the inlet (m/s)

REFERENCES

Abouzar E., Mohammad S. S. and Ali Nouri-Borujerdi., 2019. Hydrodynamics and acoustic performance analysis of marine propellers by combination of panel method, Journal of Applied Mathematics and Computing, 4(3), pp. 1-18. Available at: https://doi.org/10.3390/mca24030081.

Abrahamen, K., 2012. The ship as an underwater noise source, Proceedings of the 11th European conference on underwater acoustics, Edinburgh, Scotland, July 2-6, pp. 1-19. Available at https://doi.org/10.1121/1.4772953.

Bagheri, M.R. et al., 2015. Analysis of hydrodynamics and noise prediction of the marine propellers under cavitating and non-cavitating conditions, International Journal of Environmental Science and Technology, 22(5), pp.1918-1930. Available at: http://scientiairanica.sharif.edu/article_3754_c77aa56a6301e806ab4d058ca8b970e2.pdf.

Bagheri, M.R., Seif M.S. and Mehdigholi H., 2014. Numerical simulation of underwater propeller noise, Journal of Ocean, Mechanical and Aerospace science and engineering, 4, pp.1-6. Available at: https://isomase.org/JOMAse/Vol.4%20Feb%202014/4-1.pdf.

Batool Mousavi., Rahrovi A and Kheradmand S., 2014. Numerical simulation of tonal and broadband hydrodynamic noises of non-cavitating underwater propeller, Polish Maritime Research, 21, pp. 46-53. Available at: http://dx.doi.org/10.2478/pomr-2014-0029.

Boumediene, K. and Belhenniche, S.E., 2016. Numerical analysis of the turbulent flow around DTMB 4119 marine propeller, International Journal of Marine and Environmental Sciences,10(2), pp.1-5. Available at https://publications.waset.org/10003825/numerical-analysis-of-the-turbulent-flow-around-dtmb-4119-marine-propeller.

Boumediene, K., et al., 2019. Computational hydrodynamic analysis of a highly skewed marine propeller, Journal of Naval Architecture and Marine Engineering, 16, pp. 21-32. Available at: http://dx.doi.org/10.3329/jname.v16i1.38757.

Bouregba, F., et al., 2019. Effect of the blade number on the marine propeller performance, The European Physical Journal Conferences, 213(4). Available at: https://doi.org/10.1051/epjconf/201921302007.

Choi, W. et al., 2015. Turbulent-Induced Noise around a Circular Cylinder Using Permeable FW-H Method, Journal of Applied Mathematics and Physics, 3, pp.161-165. Available at: https://www.scirp.org/journal/paperinformation.aspx?paperid=53667.

Goutam Kumar Saha., Md. Hayatul Islam Maruf and Md. Rakibul Hasan. 2019. Marine propeller modeling and performance analysis using CFD tools, AIP Conference Proceedings, 2121(1). Available at: https://doi.org/10.1063/1.5115883.

Hai-peng, G. et al., 2019. Numerical investigation on the hydro-dynamic characteristics of a marine propeller operating in oblique inflow, Applied Ocean Research, 93, pp.101969. Available at: https://doi.org/10.1016/j.apor.2019.101969.

Jessup, S.D., 1989. An experimental investigation of viscous aspects of propeller blade flow. Ph.D. Dissertation, Faculty of the School of engineering and Architecture, Catholic University of America, USA. Available at: https://repository.tudelft.nl/islandora/object/uuid%3A2339c64f-0b69-48e1-a54d-625e959d7b35.

Lidtke, A.K., 2017. Predicting radiated noise of marine propellers using acoustic analogies and hybrid Eulerian-Lagrangian cavitation models, Ph.D. Dissertation, Faculty of engineering and the environment Fluid Structure Interaction Group, University of Southampton, United Kingdom. https://eprints.soton.ac.uk/413579/.

Lloyd, T., Rijpkema, D. and van Wijngaarden, E., 2015. Marine propeller acoustic mod-elling: comparing CFD results with anacoustic analogy method, Fourth International Symposium on Marine Propulsors, 2015, Austin, Texas. Available at https://www.marinepropulsors.com/proceedings/2015/WA4-2.pdf.

Mohsen, G., Hassan, G. and Jalal, M., 2017. Hydrodynamic effect on the sound pressure level around the marine propeller, Indian Journal of Geo-Marine Sciences, 46(07), pp.1477-1485. Available at: http://nopr.niscair.res.in/handle/123456789/42227.

Pan, Y. and Zhang, H.X., 2013. Numerical prediction of marine propeller noise in non-uniform inflow, China Ocean Engineering 27(1), pp. 33-42. Available at: https://ui.adsabs.harvard.edu/link_gateway/2013ChOE...27...33P/doi:10.1007/s13344-013-0003-2.

Seol, H., et al., 2005. Development of hybrid method for the prediction of underwater propeller noise. Journal of Sound Vibration, 288 (1-2): 345-360. Available at: https://doi.org/10.1016/j.jsv.2005.01.015.

Sezen, S. and Bal, S., 2019. A computational investigation of noise spectrum due to cavitating and non-cavitating propellers, Proceedings of the Institution of Mechanical Engineers part M: Journal of Engineering for the Maritime Environment, pp 1-14. Available at: https://doi.org/10.1177%2F1475090219892368.

Sezen, S., Dogrul, A. and Bal, S., 2017. Tip vortex index (TVI) technique for inboard propeller noise estimation. GMO, Journal of Ship and Marine Technology, 23(207), 27-37. Available at: https://pure.strath.ac.uk/ws/portalfiles/portal/88819401/Sezen_etal_GMO_2019_Tip_vortex_index_TVI_technique_for_inboard_propeller_noise.pdf.

Soydan., A., Zafer, B. and Bal, S., 2019. Investigation of underwater noise characteristics of DTMB4119 propeller under different conditions, Proceedings of the 10th Ankara International Aerospace Conference, Ankara, Turkey, September 18-20. Available at: http://aiac.ae.metu.edu.tr/paper.php/AIAC-2019-068.

Wu, Y. et al., 2019. A novel aerodynamic noise reduction method based on improving spanwise blade shape for electric propeller aircraft, Journal of Aerospace Engineering, 2019, pp. 1-10. Available at: https://doi.org/10.1155/2019/3750451.